DAA/ Langley

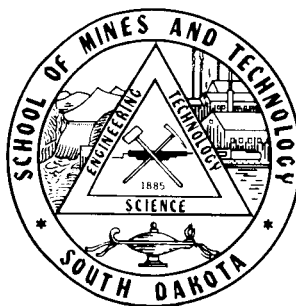**Report SDSMT/IAS/R-86/07**   September 1986

ATMOSPHERIC ELECTRICAL MODELING IN SUPPORT
OF THE NASA F106 STORM HAZARDS PROJECT:
ANNUAL REPORT COVERING THE PERIOD
15 MARCH 84 - 14 MARCH 86

By: John H. Helsdon

Prepared for:

National Aeronautical
  and Space Administration
Langley Research Center
Hampton, VA 23665

Under Grant No. NAG-1-463

Institute of Atmospheric Sciences

South Dakota School of Mines and Technology

Rapid City, South Dakota 57701-3995

Report SDSMT/IAS/R-86/07   September 1986

ATMOSPHERIC ELECTRICAL MODELING IN SUPPORT
OF THE NASA F106 STORM HAZARDS PROJECT:
ANNUAL REPORT COVERING THE PERIOD
15 MARCH 84 - 14 MARCH 86

By: John H. Helsdon

Prepared for:

Institute of Atmospheric Sciences

South Dakota School of Mines and Technology

Rapid City, South Dakota 57701-3995

TABLE OF CONTENTS

LIST OF FIGURES

LIST OF TABLES

1. INTRODUCTION

With the use of composite (non-metallic) materials and microelectronics becoming more prevalent in the construction of both military and commercial aircraft, the control systems have become more susceptible to damage or failure from electromagnetic transients. One source of such transients is the lightning discharge. In order to study the effects of the lightning discharge on the vital components of an aircraft, NASA Langley Research Center has undertaken a Storm Hazards Program in which a specially instrumented F106B jet aircraft is flown into active thunderstorms with the intention of being struck by lightning. The overall purpose of the program is to enhance the capability of detecting and avoiding the hazards associated with severe storms and improving design capabilities to protect aircraft systems from unavoidable hazards.

One of the specific purposes of the program is to quantify the environmental conditions which are conducive to aircraft lightning strikes. To this end, the F106, through 1985, has made 1378 penetrations at altitudes ranging from 3.1 km up to 12.2 km (temperatures from +5°C to -55°C) and obtained at least 690 direct strikes to the airframe (Fisher, et al., 1986). Most of the strikes have occurred at altitudes in excess of 6 km and temperatures colder than -20°C. Thus, a good data base has been established for the study of lightning interaction and environment at higher (colder) altitudes (temperatures). Analysis of these data has shown that the greatest risk of a lightning strike to an airplane occurs at altitudes between 11 and 11.6 km (-40 to -45°C) where turbulence and precipitation intensities were classified as light (Fisher and Plumer, 1984). Analysis of UHF radar observations made during flight operations has indicated that these high altitude lightning strikes were triggered by the aircraft (Mazur et al., 1984).

The results from the Storm Hazards Program are in conflict with compilations of data concerning inadvertent lightning strikes to aircraft which show that most reported strikes occur in the vicinity of 4.5 km altitude, which has been very near the freezing level. Fisher and Plumer (1984) also state that the nature of the high altitude lightning strikes encountered (triggered) by the F106 have been generally of a low amplitude current nature, consistent with the known characteristics of intracloud lightning discharges (although some of the time-resolved characteristics appear to be different than anticipated). They state the need for a larger data base for the analysis of lightning and strike characteristics at lower altitudes where these characteristics are anticipated to be somewhat different. The primary difficulty during the 6 field seasons of the F106 program has been the paucity of lightning strikes at altitudes below 6 km. To date, only 75 direct strikes to the aircraft have been recorded below 6 km, 11% of the total, with 41 of these 75 occurring in the 1985 field season alone. Virtually all of these strikes occurred in the altitude range

from 4.3 to 6 km (temperatures colder than 0°C) and were apparently triggered by the aircraft (a deduction based on the on-board sensors and UHF-band radar data).

Given the need of obtaining a better data base on lower altitude lightning strikes, an effort was undertaken to determine possible methods of directing the F106 into lower altitude regions of thunderstorms where the probability of a lightning strike would be maximized. This effort involved the work of two organizations, the Institute of Atmospheric Sciences (IAS) at the South Dakota School of Mines and Technology and Electro Magnetic Applications, Inc. (EMA) of Denver, Colorado. This report summarizes the work accomplished by IAS personnel.

2. OBJECTIVES

The objectives of this research program involved the use of the IAS two-dimensional, Storm Electrification Model (SEM) to simulate the thunderstorm environment in which the F106 was operating. The results of the model simulations would be used in two ways. The first use of the model results was to provide EMA with data on the time evolution and spatial patterns of the electric fields, small ion concentrations, electric charges on cloud and precipitation particles, and the total charge patterns in the simulated cloud. EMA personnel would then use these data as initial and boundary values in their modeling studies of the aircraft lightning environment.

The main use of the IAS model simulations was to analyze the results with an emphasis on looking for relationships between the electrical structure of the storm and the basic cloud structure. The intent of this analysis was to determine what observable character-istics of the cloud correlate with strong electric field regions at lower altitudes in the hope of devising a scheme for vectoring the F106 into such regions to increase the lightning strike probability.

An additional objective of the research effort was to develop a lightning parameterization scheme for incorporation into the SEM. The SEM, in its original configuration, was only capable of simulating the development of the electrical aspects of a thunderstorm up to the time of first lightning. Without a scheme for simulating lightning, the buildup of the electric fields and charges would continue without limit, reaching unrealistic values and causing the simulation to terminate because of the necessity of reducing the model time step in order to maintain numerical stability of the electrical transport equations in these high electric fields. In nature, the electrical stresses that build up as the charge separation processes proceed and the electric field increases are relieved by the charge transfer that accompanies the lightning discharge. An analogue to the lightning discharge must be incorporated in the model in order to accomplish the charge transfer and relief of electric stress so that simulations may continue into the mature and decaying stages of thunderstorm evolution. Only in this fashion can the complete evolution of a thunderstorm be studied dynamically, microphysically, and electrically.

3. MODEL DESCRIPTION

3.1 The Base Model

The theoretical framework is a deep-convection, slab-symmetric, two-dimensional, time-dependent (2DTD) cloud model which has been applied in the past to several atmospheric convective situations. Atmospheric wind, potential temperature, water vapor, cloud liquid and ice, rain, snow, and graupel/hail (in the form of ice pellets, frozen rain, graupel, and small hail) are the main dependent variables. The model has been developed from the works of Orville (1965), Liu and Orville (1969), Wisner et al. (1972), Orville and Kopp (1977), and Lin et al. (1983). A density-weighted stream function has been used to extend the model to deep convection.

The nonlinear partial differential equations constituting the base model include the first and third equations of motion (from which a vorticity equation is derived), a thermodynamic equation, and water conservation equations (for the three phases). The model has been designed such that mesoscale convergence can be superimposed in the lower levels and divergence in the upper levels. The manner in which such convergence is applied to the model and further details of the hydrodynamic equations can be found in Chen and Orville (1980).

The bulk-water parameterization used in this model divides water and ice hydrometeors into five classes: cloud water, cloud ice, rain, snow, and high density precipitating ice (graupel/hail) with exponential size distributions hypothesized for the three precipitating classes. Figure 1 with an accompanying key in Table 1 shows the primary cloud microphysical processes simulated in the model. Briefly, the production of rain from cloud water is simulated using equations based on the works of Kessler (1969) and Berry (1968). Graupel/hail is generated by the aggregation of snow, by the capture of snow or cloud ice by raindrops (contact freezing), or by the probabilistic freezing of raindrops (Bigg, 1953) due to the inherent ice nuclei content of a specific volume of water at suitably cold temperatures. An approximation to the Bergeron-Findeisen process is used to transform some of the cloud water to snow. Growth of hail is governed by equations for wet and dry growth (Musil, 1970) and shedding of rain from hail is included. Cloud water may be transformed to cloud ice in the region between 0°C and -40°C using an equation developed by Saunders (1957). Natural cloud ice is normally initiated at temperatures of -20°C and colder, using an equation after Fletcher (1962) for the number of natural ice nuclei active. Homogeneous freezing occurs at -40°C. Accretional processes (including riming) involving the various forms of liquid and solid hydrometeors are simulated.

Rain, snow, and graupel/hail have appreciable terminal fall velocities, while cloud water and cloud ice have zero terminal velocity and, hence, follow the airflow. Evaporation of all forms of hydrometeors

4

(THIS PAGE INTENTIONALLY LEFT BLANK)

TABLE 1

Key to Figure 1

| Symbol	Meaning
P_{IMLT}	Melting of cloud ice to form cloud water, $T \geq T_0$.
P_{IDW}	Depositional growth of cloud ice at expense of cloud water.
P_{IHOM}	Homogeneous freezing of cloud water to form cloud ice.
P_{IACR}	Accretion of rain by cloud ice; produces snow or graupel depending on the amount of rain.
P_{RACI}	Accretion of cloud ice by rain; produces snow or graupel depending on the amount of rain.
P_{RAUT}	Autoconversion of cloud water to form rain.
P_{RACW}	Accretion of cloud water by rain.
P_{REVP}	Evaporation of rain.
P_{RACS}	Accretion of snow by rain; produces graupel if rain or snow exceeds threshold and $T < T_0$.
P_{SACW}	Accretion of cloud water by snow; produces snow if $T < T_0$ or rain if $T \geq T_0$. Also enhances snow melting for $T \geq T_0$.
P_{SACR}	Accretion of rain by snow. For $T < T_0$, produces graupel if rain or snow exceeds threshold; if not, produces snow. For $T \geq T_0$, the accreted water enhances snow melting.
P_{SACI}	Accretion of cloud ice by snow.
P_{SAUT}	Autoconversion (aggregation) of cloud ice to form snow.
P_{SFW}	Bergeron process (deposition and riming) - transfer of cloud water to form snow.
P_{SFI}	Transfer rate of cloud ice to snow through growth of Bergeron process embryos.
P_{SDEP}	Depositional growth of snow.
P_{SSUB}	Sublimation of snow.
P_{SMLT}	Melting of snow to form rain, $T \geq T_0$.
P_{GAUT}	Autoconversion (aggregation) of snow to form graupel.
P_{GFR}	Probabilistic freezing of rain to form graupel.
P_{GACW}	Accretion of cloud water by graupel.
P_{GACI}	Accretion of cloud ice by graupel.
P_{GACR}	Accretion of rain by graupel.
P_{GACS}	Accretion of snow by graupel.
P_{GSUB}	Sublimation of graupel.
P_{GMLT}	Melting of graupel to form rain, $T \geq T_0$. (In this regime, P_{GACW} is assumed to be shed as rain.)
P_{GWET}	Wet growth of graupel; may involve P_{GACS} and P_{GACI} and must include P_{GACW} or P_{GACR}, or both. The amount of P_{GACW} which is not able to freeze is shed to rain.

6
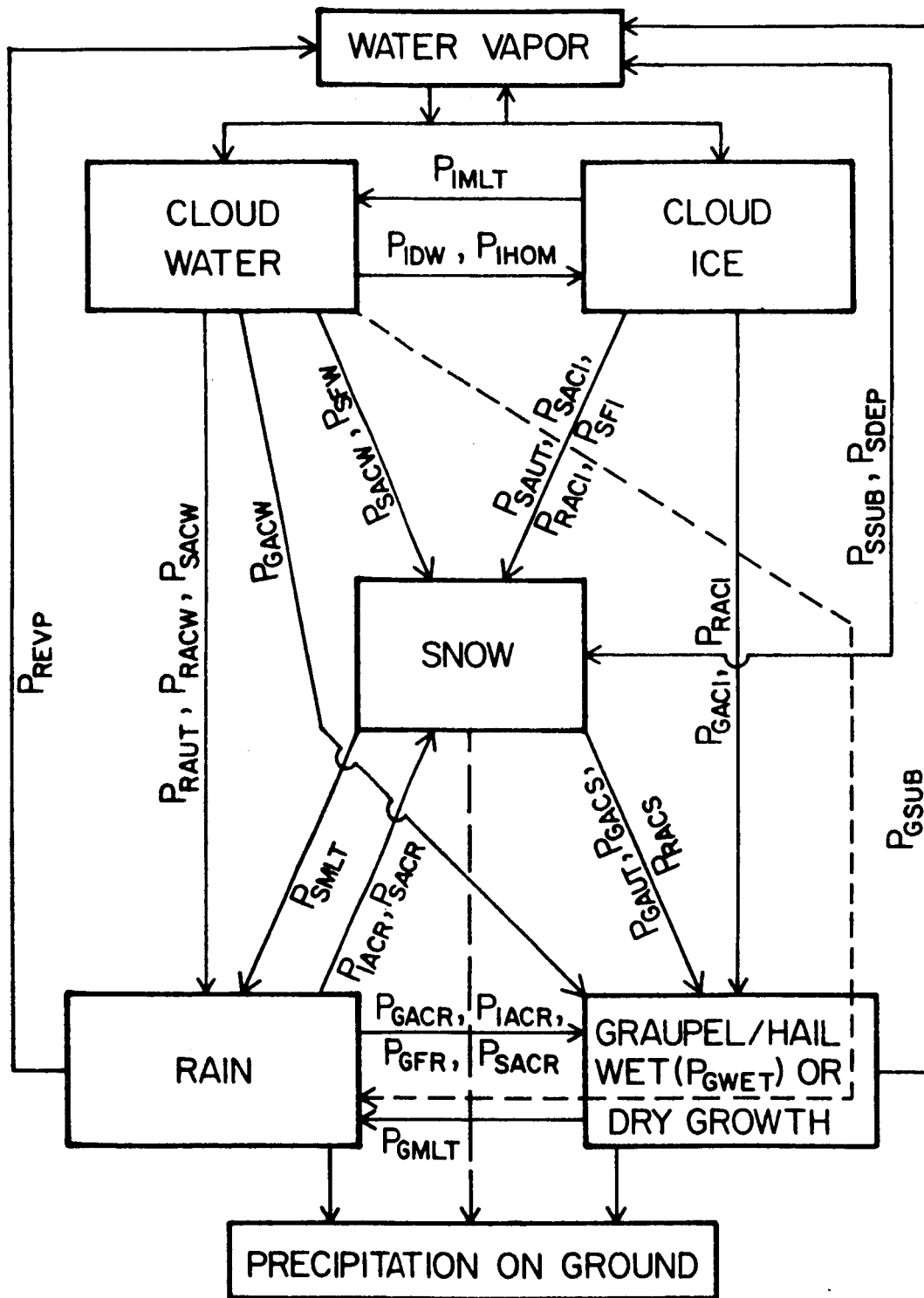
Fig. 1: Cloud physics processes simulated in the model. See Table 1 for an explanation of the symbols.

and the melting of snow and graupel/hail are also simulated. For a more detailed discussion of this model, the reader is referred particularly to Orville and Kopp (1977) and Lin et al. (1983).

3.2 The Electrical Model

This base has been modified to include various processes involved in thundercloud electrification. These modifications involved the coupling of the electro-microphysical processes which account for the charge exchange between interacting particles within the cloud domain. The means of coupling the electro-microphysics to the dynamics and microphysics of the base model are based on ideas from Chiu (1978), Helsdon (1980), and Kuettner et al. (1981). Each of the five classes of hydrometeors is allowed to have a charge associated with it. This charge is then transported with the species of hydrometeor according to the general equation

$$\frac{\partial Q}{\partial t} = -\vec{V} \cdot \nabla Q + \frac{1}{\rho_a} \frac{\partial}{\partial z} (U_t Q \rho_a) + \nabla \cdot K_m \nabla Q \pm \left(\frac{\delta Q}{\delta t}\right)_{inter} \quad , \quad (1)$$

where Q represents the charge density (C m^{-3}) carried by the hydrometeor class (positive or negative), $\vec{V}$ is the 2D velocity vector, ρ_a is the air density, U_t is the mass-weighted mean terminal fall speed of the hydrometeor class, K_m is the nonlinear eddy coefficient and $(\delta Q/\delta t)_{inter}$ represents the charge exchanged between classes of hydrometeors due to interactions. The first term on the right is the advection term, the second is the fallout term (zero for cloud water and cloud ice charge), and the third is the eddy mixing term. The last term in (1) will be discussed below.

The model framework accounts for the presence of small ions as well. The equation governing the number concentration of small ions is

$$\frac{\partial n_{1,2}}{\partial t} = -\nabla \cdot [n_{1,2}\vec{V} \pm n_{1,2}\mu_{1,2}\vec{E} - K_m \nabla n_{1,2}] + G - \alpha n_1 n_2 + Src - Sink. \quad (2)$$

Here $n_{1,2}$ is the concentration of small ions (the subscript 1 representing positive ions and 2 the negative ions); μ is the small ion mobility (m^2 V^{-1} sec^{-1}, pressure dependent); $\vec{E}$ is the 2D electric field vector; G is the ion generation rate due to cosmic ray ionization (ions m^{-3} sec^{-1}, dependent on height); α is the ion-ion recombination coefficient (1.6×10^{-12} m^3 sec^{-1}); Src is the source term for small ions from processes other than cosmic ray ionization; and $Sink$ is the sink term for small ions from processes other than recombination. An example of a source process for small ions would be the evaporation of a charged hydrometeor, while a sink process would be Wilson capture (ion attachment to hydrometeors).

With the various types of charges accounted for in the model, a total charge density can be diagnosed at each grid point from

$$\rho = e(n_1 - n_2) + \Sigma Q \quad , \tag{3}$$

where ρ is the total charge density ($C\ m^{-3}$) and e is the electronic charge (1.6×10^{-19} C). The first term represents the net charge due to the difference in small ion concentrations and the last term represents the net charge on the five classes of hydrometeors. With the net charge determined, we then use Poisson's equation

$$\nabla^2 \phi = \rho / \varepsilon \tag{4}$$

to determine the scalar electric potential, ϕ (Volts). In (4), ε is the electrical permittivity of air ($8.86 \times 10^{-12}\ kg^{-1}\ m^{-2}\ sec^2\ C^2$). Finally, the 2D electric field vector can be determined from the potential via Gauss's law

$$\vec{E} = -\nabla \phi \quad . \tag{5}$$

The last term in (1) represents the charge exchanged between any two classes of hydrometeors during an interaction between those two classes. Such interactions may be accretional or non-accretional in nature. It should be noted that, in such interactions as P_{iacr} in Fig. 1 (Table 1), where cloud ice is nucleating rain to form snow, the charge on the cloud ice and rain are summed and the total is introduced into the snow charge resulting in a three bodied type of transfer.

In the collisional process where a finite separation probability exists, two types of electrical interactions are possible: inductive processes, where the ambient electric field strength and its orientation with respect to the particles influence the magnitude and sign of the charge transfer; and non-inductive processes, where the ambient field exerts no influence, but such factors as temperature, liquid water content, and impact speed determine the charge transfer. The model has been configured to allow for the accounting of both inductive and non-inductive processes either individually or in concert. This is accomplished by starting with the following representation of the charge transferred between two interacting particles,

$$\Delta q = \Delta Q + 4\pi\varepsilon\gamma_1 |\vec{E}| \cos(\vec{E}, \vec{r}_{LS}) r_s^2 + Aq_L - Bq_S \quad , \tag{6}$$

9

where ΔQ is the charge transferred due to any non-inductive process, γ_1 is a dimensionless variable which depends on the ratio of the radii of the two interacting particles, $\vec{r}_{LS}$ is the vector along the line joining the centers of the two particles at the time of impact, r_S is the radius of the smaller particle, q_L (q_S) is the charge already existing on the large (small) particle and A (=1-B) is a dimensionless variable which depends on the radius ratio of the two hydrometeors. The first term, then, represents the non-inductive charge transfer, while the second term represents the inductive transfer. The last two terms account for the effect of charge already residing on the hydrometeors. Switches are used to activate/deactivate either process.

A single large hydrometeor may interact with many smaller particles in a unit time, so we integrate over the volume swept out by the large particle

$$\frac{\partial q_L}{\partial t} = \int E_f |\vec{V}_{SL}| N_S \Delta q S(\alpha) dA \tag{7}$$

to obtain the charge acquired per unit time by the large particle. In (7), E_f is the collision efficiency between the two particles, $|\vec{V}_{SL}|$ is the relative impact speed, N_S is the number concentration of the smaller particles, Δq comes from (6), and $S(\alpha)$ is the angle-dependent separation probability. The integration results in three possible charging rates for the larger hydrometeor depending on which charge transfer mechanisms are active

$$\frac{\delta q_L}{\delta t} = C_1 \left\{ C_2 + Bq_S - Aq_L \right\} \quad , \tag{8}$$

where $C_1 = E_f |\vec{V}_{SL}| N_S \pi r_L^2 <S>$ (r_L being the radius of the large particle and $<S>$ is the mean separation probability) and

$$C_2 = \begin{cases} -\Delta Q & \text{non-inductive,} \\[2ex] 4\pi\epsilon\gamma_1 |\vec{E}| \cos(\vec{E},\vec{V}_{SL}) r_S^2 <\cos\alpha> & \text{inductive,} \\[2ex] 4\pi\epsilon\gamma_1 |\vec{E}| \cos(\vec{E},\vec{V}_{SL}) r_S^2 <\cos\alpha> - \Delta Q & \text{combined.} \end{cases} \tag{9}$$

Note that in (9) there are two important angles influencing the charge exchange: 1) the angle between the electric field vector and relative velocity vector of the two particles $[\cos(\vec{E},\vec{V}_{SL})]$ and 2) the average collision contact angle ($<\cos\alpha>$). For all practical purposes, the quantity $|\vec{E}| \cos(\vec{E},\vec{V}_{SL})$ is adequately approximated by $-E_z$, the negative of the vertical electric field component.

10

Since (8) implies that multiple charging interactions are possible for a precipitating hydrometeor per unit time of fall, and since the charge on the large particle appears on the right-hand side of the equation, it is not safe, a priori, to assume that $\delta q_L / \delta t$ is constant over a given time step. To account for this, we integrate (8) over the length of a time step, Δt, to obtain the charge transferred to the larger particle assuming that all quantities on the right-hand side are constant except q_L. This may seem like a contradiction at first since both the electric field, $|\vec{E}|$, and the charge on the small particles, q_S, appear on the right-hand side and would seem to be subject to time variation as well. It is safe to assume the constancy of q_S, since it is highly unlikely that any one cloud droplet or ice crystal will undergo more than one non-accretional collision per time step. In the case of the electric field strength, it is a much more macroscopic quantity, being determined by the entire charged volume of the cloud and not so significantly by the local charge changes exhibited by individual particles, although the effects of local volumes dominate. In spite of this, we do admit that the field can change rapidly on a local scale, but one other factor exists to help substantiate our locally steady assumption. This is the fact that the time step in the model is dependent on the electric field strength through the field's interaction with the small ion flux term. In order to maintain the stability of the ion transport equations, the time step must be reduced as the field strength increases. By the time the electric field has reached significant levels, the time step has been reduced to values of one second or less. Thus, we apply the steady field assumption with some confidence.

Carrying out the integration of (8) results in the following expression for the charge accumulated by a precipitating hydrometeor during a time step Δt,

$$\Delta q_L = (Q_m - q_{L0})\left(1 - e^{-\Delta t/\tau_1}\right) \quad , \tag{10}$$

where q_{L0} is the initial charge on the large particle, and the parameters Q_m and τ_1 are given by

$$Q_m = \begin{cases} (-\Delta Q + Bq_S)/A & \text{non-inductive,} \\ (4\Pi\epsilon\gamma_1\cos(\vec{E},\vec{V}_{LS})r_S^2\langle\cos\alpha\rangle + Bq_S)/A & \text{inductive,} \\ (4\Pi\epsilon\gamma_1\cos(\vec{E},\vec{V}_{SL})r_S^2\langle\cos\alpha\rangle - \Delta Q + Bq_S)/A & \text{combined,} \end{cases} \tag{11}$$

and

$$\tau_1 = (E_f|\vec{V}_{SL}|N_S\pi r_L^2\langle S\rangle A)^{-1} \quad . \tag{12}$$

Finally, the charge accumulated by one precipitating hydrometeor is multiplied by N_L, the number concentration of the large particles, in order to arrive at the total charge density created by interactions, which appears as part of the last term in (1). The other components of the last term in (1) include the accretional terms, evaporational processes, and ion attachment processes. Examples of the formulation of the attachment and accretional processes are available in Chiu (1978) and Helsdon (1980).

3.2.1 Charging processes

A great deal of laboratory and theoretical work has been, and continues to be done to investigate possible mechanisms of charge separation. A non-exhaustive list of possible mechanisms includes: 1) selective ion capture (Wilson, 1929); 2) convective charging (Vonnegut, 1955); 3) induction charging involving non-accretional collisions between various classes of particles in the electric field (Sartor, 1961, 1967, 1981; Muller-Hillebrand, 1954; Paluch and Sartor, 1973); 4) effects of freezing potentials during wet growth of hail or splashing collisions between graupel and raindrops (Workman and Reynolds, 1948, 1950; Latham and Warwicker, 1980; Shewchuk and Iribarne, 1971); 5) non-inductive charging during the riming of graupel (Reynolds et al., 1957; Buser and Aufdermaur, 1977; Takahashi, 1978; Gaskell and Illingworth, 1980; Jayaratne et al., 1983); 6) riming of graupel followed by splintering (Latham and Mason, 1961; Hallett and Saunders, 1979); and 7) evaporative charging of ice crystals in penetrative downdrafts (Telford and Wagner, 1979). It is entirely possible that all of these mechanisms (or some as yet undiscovered mechanism) are active to one degree or another in various thunderstorm situations. However, in order to minimize the degree of complexity involved in the modeling work, it was necessary to limit the mechanisms included in the model to a workable set.

The basic charge separation mechanisms included within the model can be broken down into four basic categories:

1) Graupel interacting with particles in a dry growth mode.

2) Graupel interacting with particles in a wet growth mode.

3) Rain interacting with cloud droplets.

4) Small ions interacting with all classes of hydrometeors.

Within these various categories, the two types of electrical interactions discussed above may be possible, i.e., inductive and/or non-inductive transfers.

The inductive water-water charge transfer interaction is generally believed to be ineffective in producing electrification typical of thunderstorm conditions on its own. Jennings (1975) has shown that such a process is capable of producing early electrification in clouds with fields up to 30 kV/m being possible. After this threshold is

12

reached, the mechanism extinguishes itself due to the presence of such a field causing all collisions to result in permanent coalescence. This ability to generate early electrification well below thunderstorm values, but significantly above the background fair weather field, may affect the nature of other electrification mechanisms which must await the formation of ice particles for their initiation.

The charge separation resulting from the interaction of liquid drops and ice particles may be of a non-inductive or inductive nature. Kuettner et al. (1981) have summarized the controversy regarding the action of a non-inductive, ice-water charging mechanism. They chose to include such a process in their model (using conservative values for the charge transferred per collision) based on the lack of conclusive evidence for eliminating the mechanism and the fact that the riming process is a well established microphysical phenomenon in thunderclouds.

The non-inductive, ice-ice process is the subject of as much controversy as the water-ice mechanism; however, the controversy does not center around whether the process is effective, but rather exactly what physical mechanism is responsible for the charge exchange and, to a lesser degree, the magnitude of the charge transferred. Results have been summarized and assessed by Gross (1982).

The inductive mechanisms involving water-ice and ice-ice interactions have been argued as being ineffective in nature because only grazing collisions near the electrical equator result in separation of particles and charge in the ice-water case, and because of a relaxation time limitation on charge migration in the ice-ice case. In the ice-water case, it is true that grazing collisions will result in minimal charge separation; however, Sartor (1981) has shown that, due to the surface roughness of graupel particles, cloud droplets can bounce off of such rough particles from almost any impact angle negating the above restriction. In the ice-ice case, the relaxation factor may be included in the formulation, and the mechanism's importance may be tested without great difficulty. In addition, the results of Tzur and Levin (1981) and Kuettner et al. (1981) have indicated that the combination of inductive and non-inductive mechanisms involving the ice phase yield the most realistic results.

With this discussion in mind and referring to Fig. 1 and Table 1 for the interactions listed below, the model in its present configuration can account for both inductive and non-inductive charge transfers when rain (P_{gacr}), cloud ice (P_{gaci}), and snow (P_{gacs}) interact with graupel in category (1). In category (2), graupel can interact with rain and cloud water (P_{gacr} and P_{gacw} through P_{gwet}) with the result that excess water is shed as rain (the wet growth process). In this category, only inductive charge transfers are accounted for due to uncertainty about the actual microphysical interactions taking place. This category is under further development at this time with a formulation for a non-inductive transfer

13

being devised. In category (3), a limited inductive mode transfer is allowed. In addition, both inductive and non-inductive charge transfers are allowed when cloud ice interacts with snow. The category (4) interactions involving small ions have been described above.

3.3 Initialization

3.3.1 Environmental initialization

The base state of the atmosphere for this model is taken from a rawinsonde sounding typical of the type of day being studied. This sounding of temperature and moisture is, hopefully, representative of the atmosphere near the time of the formation of an observed cloud which may be compared with the model simulation, if such observations are available. The only modification made to the original sounding is to make the lowest layer adiabatic (if it is not already in such a state). The atmospheric winds are determined by projecting the winds from the sounding in the direction of the storm motion, since the model is two-dimensional. In addition, the winds determined by this procedure are frequently reduced to some percentage of their original value because the use of full winds has a tendency to propagate the simulated cloud off the grid too rapidly. Dynamically, this approach is not on firm ground, and it would be better to subtract a mean wind from the actual winds and thus allow the model domain to translate. This approach will be incorporated in future work.

In order to initiate convection, we use a combination of random perturbations in temperature and water vapor in the lower 3 km of the grid (with maximum amplitude $\pm 0.5°C$ and $\pm 7\%$) and a warm bubble in the vicinity of the domain center. The bubble has a maximum deviation of $1.5°C$, is 4.8 km wide, and is present between 400 m and 2 km height.

3.3.2 Electrical initialization

We assume that an initial steady state exists with ion production due to cosmic ray generation, ion loss due to recombination, and ion transport due to conduction in the ambient electric field all balancing. We ignore ionic diffusion and invoke horizontal homogeneity so that the initial values of the variables are functions of height only. Then the aforementioned steady state balance can be described by

$$\frac{d}{dz} (\mu_1 n_1 E_z) = G(z) - \alpha n_1 n_2 \qquad (13a)$$

and

$$\frac{-d}{dz} (\mu_2 n_2 E_z) = G(z) - \alpha n_1 n_2 \quad . \tag{13b}$$

The terms in these equations have been previously defined. E_z is the assumed fair weather electric field profile patterned after Gish (1944) which exhibits an exponential decrease with height such that

$$E_z = E_0[b_1 \exp(-a_1 z) + b_2 \exp(-a_2 z) + b_3 \exp(-a_3 z)] \quad . \tag{14}$$

In (14), the parameters E_0, b_i, and a_i are varied to adjust the vertical profile. This vertical electric field profile can be related to the small ion densities by

$$\frac{dE_z}{dz} = \frac{e(n_1 - n_2)}{\varepsilon} \quad . \tag{15}$$

We subtract Eq. (13b) from (13a) and integrate in the vertical to obtain

$$e(\mu_1 n_1 + \mu_2 n_2) = \lambda_T E_z = J_c \quad , \tag{16}$$

where λ_T is the total conductivity of the air and J_c (A m^{-2}) is the fair weather air-earth conduction current, which is assumed constant with height. Equations (15) and (16) can be solved simultaneously for n_1 and n_2 yielding

$$n_1 = \left(\frac{J_c}{E_z} + \mu_2 \varepsilon E_z' \right) \frac{1}{e(\mu_1 + \mu_2)} \tag{17a}$$

and

$$n_2 = n_1 - \frac{\varepsilon E_z'}{e} \quad . \tag{17b}$$

If we assume, following Shreve (1970), that the polar ionic mobilities vary exponentially with height such that

$$\mu_{1,2} = c_{1,2}\exp(\beta z) \quad , \tag{18}$$

where $c_1 = 1.4 \times 10^{-4}$ and $c_2 = 1.9 \times 10^{-4}$ m^2 V^{-1} sec^{-1}, and $\beta = 1.4 \times 10^{-4}$ m^{-1}, then (17a) and (17b) define the initial profiles for positive and negative small ions. Finally, either (13a) or (13b) may be solved for the galactic cosmic ray generation function $G(z)$ which, after some algebraic manipulation, yields

$$G(z) = \frac{\mu_1\mu_2\epsilon}{e(\mu_1 + \mu_2)}[\beta E_z E_z' + (E_z')^2 + E_z E_z''] + \alpha n_1 n_2 \quad . \tag{19}$$

The initial fair weather electrical state of the atmosphere is determined from Eqs. (14) and (17) - (19) by choosing appropriate values of E_0, a_i, b_i, and J_c.

3.4 Boundary Conditions

The top boundary is assumed to be rigid with all variables held constant. The vorticity, vertical velocity, rain, snow, graupel, cloud water, and cloud ice as well as their associated charges are all set to zero. The stream function, entropy, water vapor mixing ratio, small ion concentration, and electric potential are maintained undisturbed at their initial values. The potential at the top of the model is obtained by integrating (5) over the depth of the domain and employing (14) for the electric field profile. This constraint on the electric potential is somewhat unrealistic and a boundary condition involving the derivative of the potential at the top is being devised.

At the lower boundary, the vertical velocity, vorticity, and stream function are set to zero. The electric potential is also set to zero, consistent with the assumption that the earth's surface is a conducting plane. Evaporation and heating rates at the surface are prescribed as functions of time. Heat and water vapor are allowed to diffuse into the lower boundary. Clouds are not permitted to form at the surface, but precipitation is allowed to fall through the surface level. Cloud shadow effects (on heating) are also simulated at the lower boundary.

At the lateral boundaries, the horizontal gradients of the stream function and the potential are assumed to be zero. Diffusional transport also assumes horizontal gradients of zero for all variables at the lateral boundaries. Both inflow and outflow from the domain are allowed. The constraints on the potential at the various boundaries result in the electric field components $E_x = 0$ at all boundaries and E_z being calculated at all boundaries.

3.5 Numerical Techniques

The equations are solved over a 19.2 km x 19.2 km domain with a
200 m grid interval in both the X and Z directions. The advection
technique used is that of Crowley (1968), which is first-order accurate
in time and second-order in space. A two-step advection scheme is used
(Leith, 1965) with vertical advection calculated first, followed by
horizontal advection. Model variables are held constant at lateral
inflow boundaries, whereas extrapolation via upstream differencing is
employed at outflow boundaries. The general purpose Helmholtz solver
in Cartesian coordinates (from the NCAR program library) is used to
solve the Poisson-type equations for stream function and electrical
potential. Centered differences are used throughout except at the
upper and lower boundaries where second order, one-sided differences
are used.

4. RESEARCH RESULTS

4.1 Wallops Island Simulation

The first use of the SEM in connection with the Storm Hazards project was to simulate the 12 September 1983 operational flight of the F106 (flight 83-053) which experienced two lightning events near 28 kft during separate cloud penetrations. This simulation is termed a blind case because there were no specific observations with which the model results could be compared for verification.

The SEM was initiated using the Wallops Island, Virginia, 00Z sounding from 13 September 1983, shown in Fig. 2, which was near the time of the flight operations (2215-2258 GMT) and was considered characteristic of the atmospheric state in which the storms were developing. The temperature has been modified in the lowest hundred millibars to make the profile adiabatic, as described in Section 3.3.1. Examination of the sounding shows that the Lifted Index is -6.7 and the K Index is 42.1, indicating a very high potential for strong thunderstorms on that day. In fact, severe thunderstorms might have been expected except for the fact that the upper level winds were quite light and exhibited little shear. Much convective activity was actually observed on that day. With this sounding as input for the model, we expected strong convection to develop.

Figure 3 shows the characteristics of the modeled storm resulting from the simulation at two different simulation times: 15 and 22.5 min. The left column contains plots at 15 min, while the right column shows the same plots at 22.5 min. The plots from top to bottom represent the dynamical and microphysical character of the cloud (see plot caption for details), radar reflectivity, vertical velocity, total charge density, vertical electric field component, and the horizontal electric field component. As is evident from Fig. 3, the model simulation of this warm based (~16°C), maritime type storm showed a very rapid development with rain formation proceeding via the stochastic coalescence process well before the ice phase became significant. Note the nearly vertical development of the storm due to the lack of wind shear.

The early charge distribution and resulting weak electric fields were a result of the limited inductive interactions between raindrops and cloud droplets. Once the ice phase appeared, the charge separation processes became more vigorous and, in the course of a few minutes, charge densities reached the order of 10's of nanocoulombs per cubic meter, accompanied by electric field strengths in excess of 400 kV/m, a value near that necessary to produce lightning breakdown. The "classic" thunderstorm dipole structure (positive charge above negative) was produced in the simulation with a lower positive charge region also in evidence, although there were no observations upon which to judge the correctness of the model results.
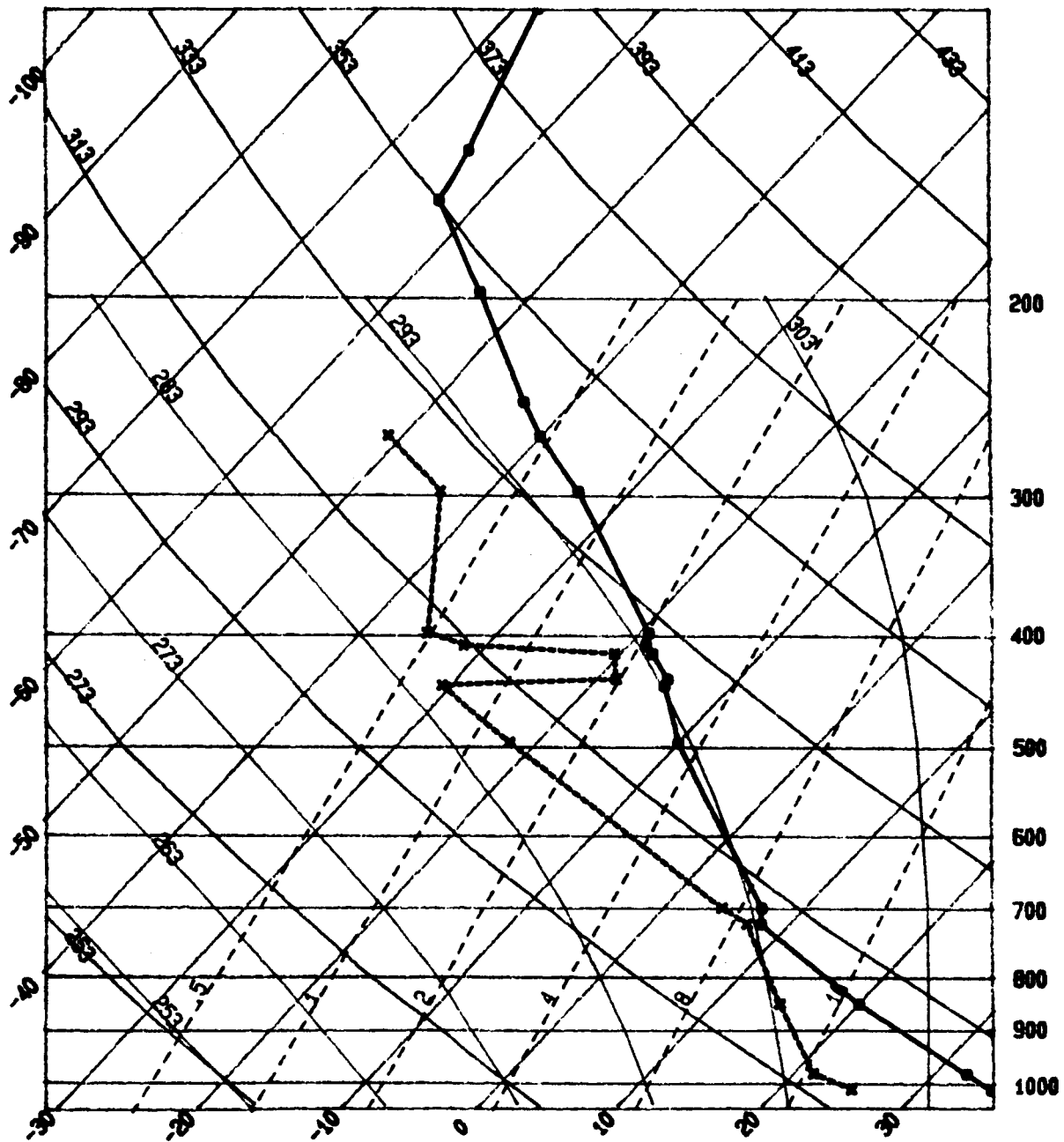
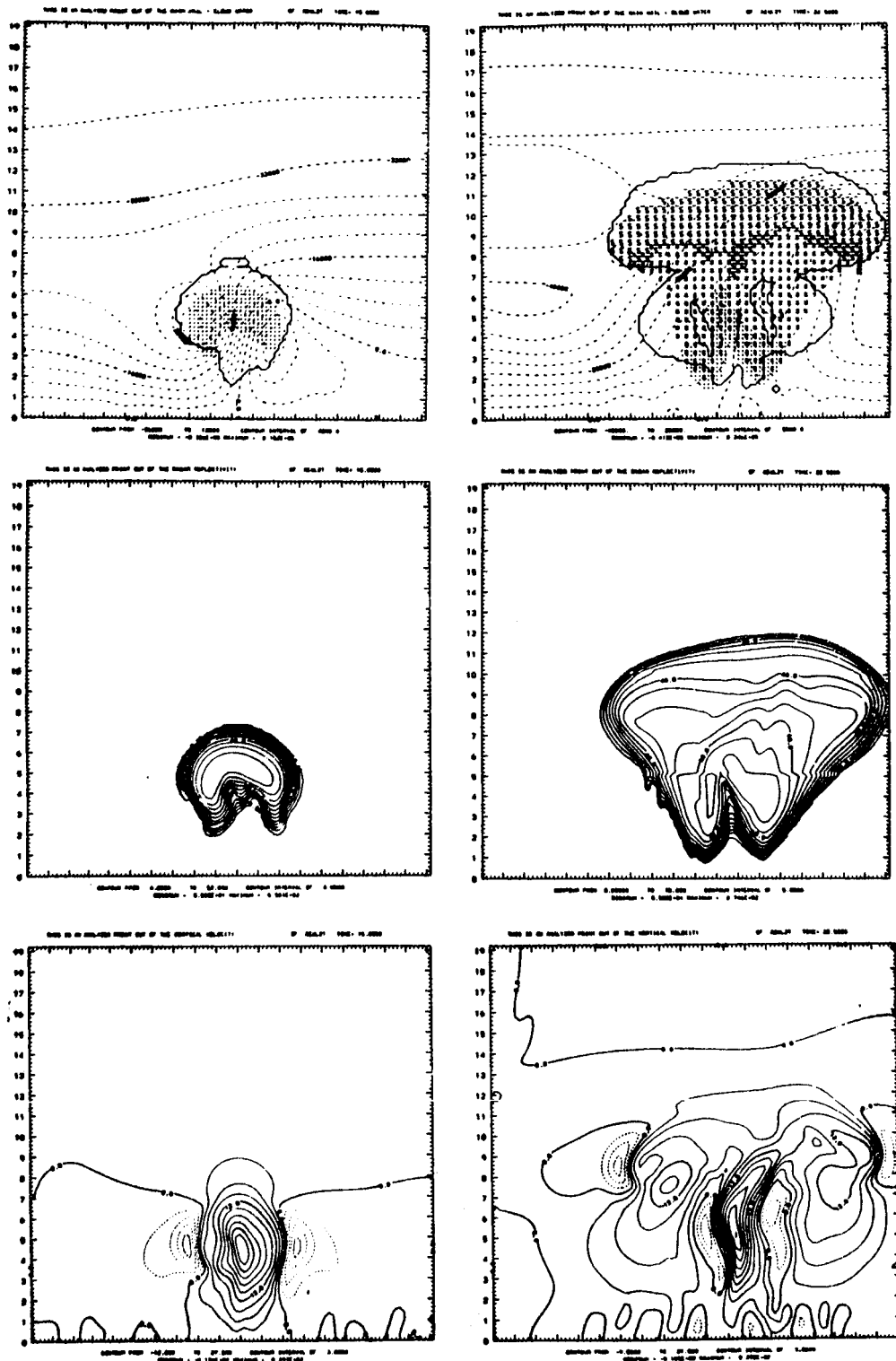**Fig. 2:** Wallops Island, VA (WAL) sounding for 00Z, 13 September 1983.

Fig. 3: Characteristics of the Wallops case for two different simulation times: left column, 15 min; and right column, 22.5 min. Reading from top to bottom, the plots represent: 1) storm dynamical and microphysical character including airflow streamlines (dashed lines), cloud boundary (solid line), and presence of snow (S), graupel (*), rain (●), and cloud ice (-) in amounts greater than a threshold value; 2) radar reflectivity in dBz (absolute values systematically too high, but structure is representative, contour interval 4 dB at 15 min, 5 dB at 22.5 min;
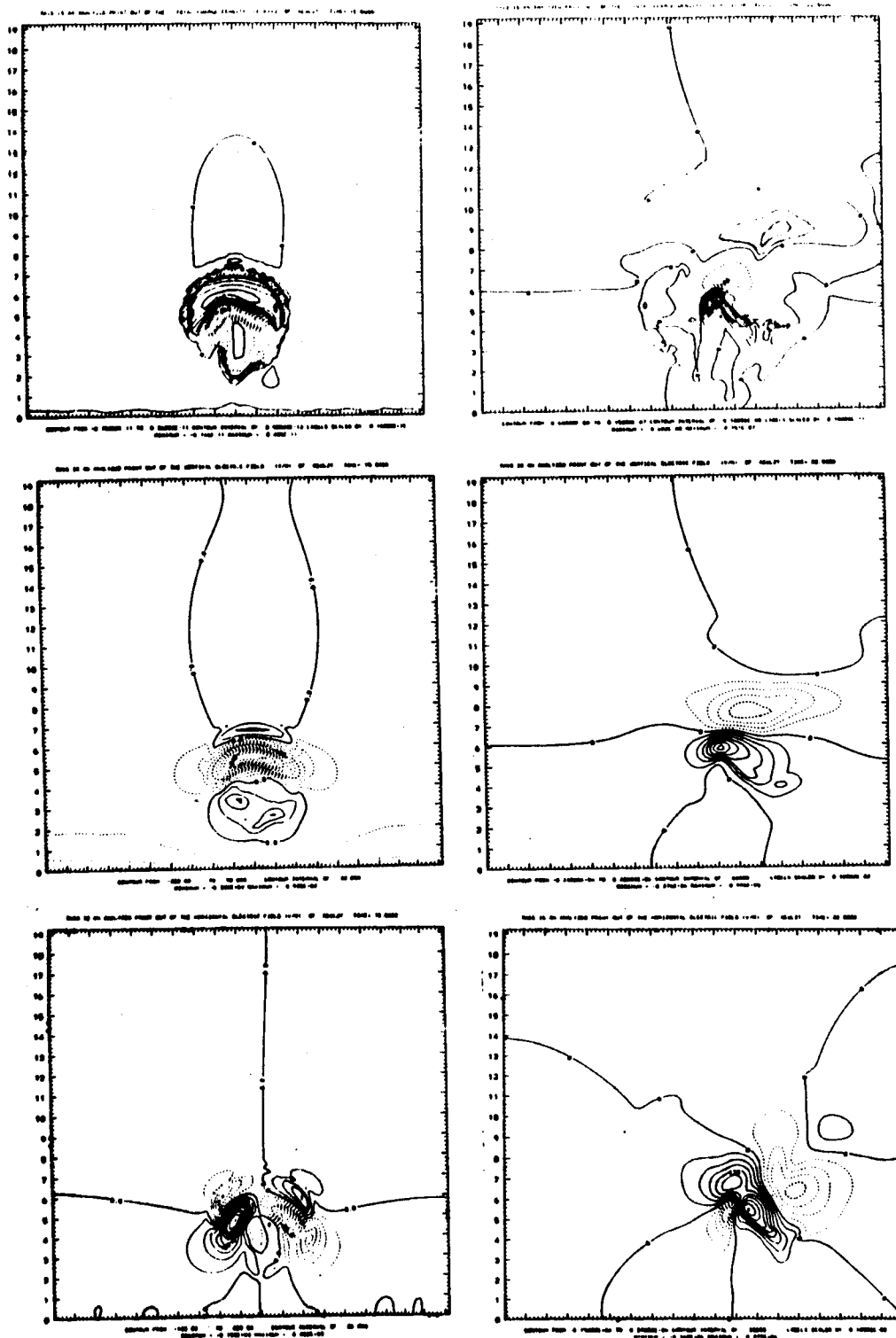
20

Fig. 3 (continued):
3) vertical velocity in m sec^{-1} (updraft-solid, downdraft-dashed, contour
interval 3 m sec^{-1}); 4) total charge density in C m^{-3} (positive-solid,
negative-dashed, contour intervals 0.9 pC.m^{-3} at 15 min, 1 nC m^{-3} at
22.5 min); 5) vertical electric field in V m^{-1} at 15 min, 60 kV m^{-1} at
22.5 min); 6) horizontal electric field (as per the vertical field,
contour intervals 20 V m^{-1} at 15 min; 30 kV m^{-1} at 22.5 min).

21

The model run for this Wallops Island case had to be terminated after 22.5 minutes of simulated real time due to the continued buildup of the electric fields and the resulting prohibitively small time steps necessary to maintain computational stability of the ion transport equations. A simulation without electrical processes active was run much longer in time. The inclusion of the lightning discharge in the model is necessary to overcome this early termination problem.

Although the electrical simulation had to be terminated prematurely, the outputs provided information on the electrical environment which might be expected during the early stages of thunderstorm development. These data in a form similar to Figs. 3 and 4, including electric fields, particle densities and charges, and ion densities at various altitudes and times within the simulated thunderstorm, were sent to EMA for use in conjunction with their 3D interaction model (Rudolph et al., 1984). The plots in Fig. 4 represent measurements which an instrumented aircraft would record if it made a level pass through the model storm at a given altitude. From these plots, EMA scientists were able to extract information considered representative of the environment in which the F106 might have operated.

Part of their work involved a determination of the shape factors due to the aircraft necessary to interpret the electric field mill data which is recorded during each F106 flight. Another aspect of their research was to do a parameter study of the aircraft under various electrical initial conditions using data from the SEM simulation, where appropriate. Their results (Rudolph and Perala, 1985), analyzing the data from the electric field mills at the time of a lightning strike to the aircraft during flight 83-053, showed that the field was predominantly vertical and negative in value. From examination of Fig. 4 at 22.5 min, the model predicts an environment in the neighborhood of 28,000 ft which is approaching conditions suitable for lightning activity (particle charges in excess of 5 nC/m^3 and electric fields approaching 300 kV/m), indicating that the model is capable of generating an environment which is similar to that which was observed.

The investigation of the low altitude strike problem is aided by looking at some of the model results. Figure 5 shows contour plots of the vertical electric field component (left panel) with solid contours indicating an upwardly directed (positive) field and dotted contours representing downwardly directed (negative) fields. The interval of each contour is 60 kV/m with the zero line indicated. The right panel represents the mixing ratio of graupel in the cloud in grams of graupel per kilogram of dry air. The contour interval in this panel is 1 g/kg. These plots represent the state of these two model variables for the Wallops Island simulation at 22.5 minutes after the initiation of the run.

The three horizontal lines drawn through the contour plots represent three possible flight altitudes for the F106. The dashed

WAL830400 13 SEP 83 0000GMT   NO SEED   AEWLO2
HAIL VARIABLES AT Z= 8.4 KM. T=22.5 MIN

WAL830400 13 SEP 83 0000GMT   NO SEED   AEWLO2
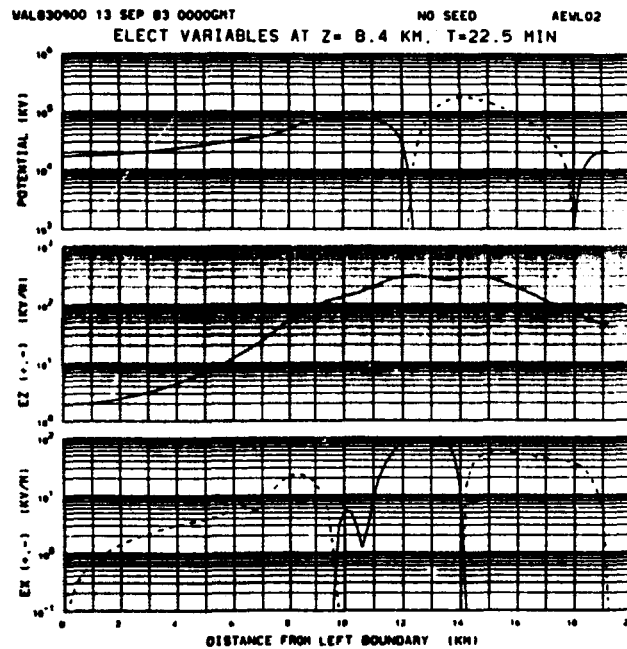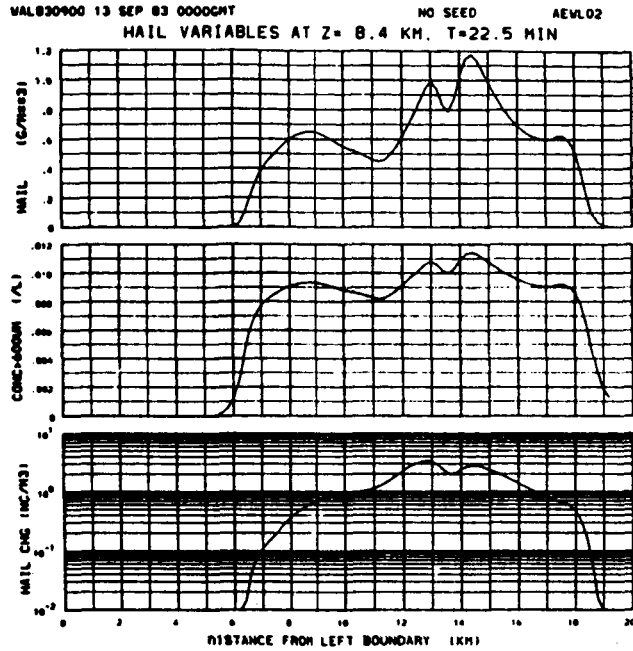ELECT VARIABLES AT Z= 8.4 KM. T=22.5 MIN

Fig. 4: Examples of measurements which would be recorded by an
instrumented aircraft flying a horizontal path through the modeled
storm at 8.4 km AGL and 22.5 min simulation time. Top plot: hail
(graupel) content in g m^{-3}, number of graupel particles ℓ^{-1} with
diameters > 600 μm, and charge on the graupel particles in nC m^{-3}
(positive charge-solid line, negative charge-dashed line). Bottom
plot: potential above ground in kV, vertical electric field com-
ponent (E_z) in dV m^{-1} (positive-solid, negative-dashed), and
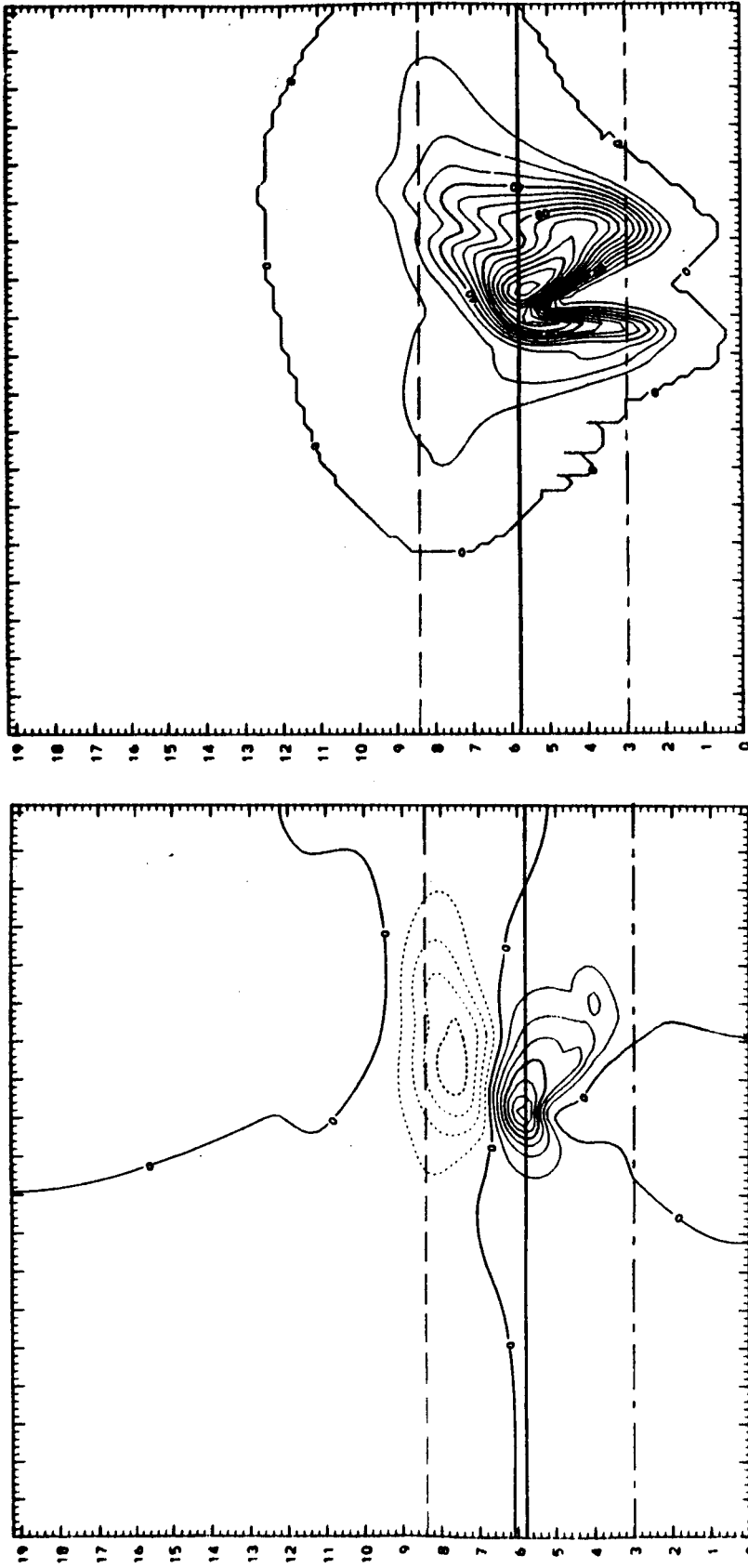horizontal field component (E_x) in kV m^{-1}.

Fig. 5: Plots from the Wallops Island simulation at 22.5 minutes showing vertical electric field component (left panel) and graupel mixing ratio (right panel) over the model domain (19.2 x 19.2 km). In the left panel, downwardly directed fields are indicated by a dotted line and upwardly directed fields are contoured with a solid line. The contour interval is 60 kV/m and the zero line is marked. In the right panel, the contour lines represent mixing ratios in grams of graupel per kilogram of dry air and the contour interval is 1 g/kg. Also represented are possible flight altitudes of the F106 at 10 kft (3 km), 19 kft (5.8 km) and 27 kft (8.4 km) [see text].

line at 8.4 km represents the altitude at which the aircraft was operating at the time of the lightning strikes. The dash-dot line represents a flight level of approximately 10 kft, and the solid line, a level of around 19 kft. (The major tick marks on the horizontal and vertical axes represent distance in kilometers). These two lower altitudes are in the region considered by program personnel to constitute the low altitude lightning environment (<20 kft).

Examination of the figure reveals that, at the altitude at which the aircraft was operating on that day, a high electric field environment would have been encountered (if the model is adequately simulating the cloud which was penetrated). The model results further indicate that had the F106 been operating in the vicinity of 10 kft, it would have encountered relatively low field strengths and probably not have been able to trigger a discharge (the triggering process seems to predominate at high altitudes). On the other hand, the flight level around 19 kft shows that a very concentrated and intense region of electric field in excess of 400 kV/m might have been encountered by the F106 had it been flying at that altitude. This result seems to indicate that lower level, high field regions could exist in the types of clouds penetrated during the project; however, examination of the right panel in the figure shows that this high field region is coincident with the maximum hail content of the storm (mixing ratio in excess of 14 g/kg). In addition, examination of Fig. 3 shows that this high field region also corresponds to a region of strong updraft and a sharp updraft/downdraft boundary, indicating the possibility of strong turbulence. Therefore, while a volume favorable to the initiation of lightning by the F106 in the low altitude region may be present, the simulation of this one case indicates that the aircraft would have to purposely avoid such a region for safety considerations. It is also interesting to note that the majority of the low altitude strikes that have occurred during the 1985 field season have been in the 15-20 kft region. This leads one to speculate that the low altitude, high field region may be a reasonably frequent feature of the storms encountered by the F106 and is not always associated with adverse flying conditions. More simulations of the electrical evolution of such clouds during their mature and dissipating stages will help to clarify this question.

These results brought to light several questions and limitations which resulted in additional research. First of all, while the model seemed to be producing realistic simulations of the storm conditions within which the F106 was operating and the data provided to EMA was useful in their analyses, we had no way of knowing whether or not the simulations were actually correct. The only way to verify the ability of a model to simulate nature is to have actual observations against which to compare the model results. The comparison between the F106 field mill data and the model output done by EMA scientists was encouraging, but was not a sufficient test. Such a test has been done on the model for a cold-based continental type storm (Helsdon et al., 1984) giving us confidence that the model can correctly simulate cloud

25

development and its attendant electrification. However, there are significant differences between cold-based, continental clouds and the warm based, maritime type clouds found along the east coast. These differences are such that we do not feel it is safe to assume that, because one type of cloud is well modeled, a different type of cloud will be equally well modeled.

Another, and even more important consideration, involves the inability of the model to simulate the electrical development of a cloud beyond its early stages. As noted above, the Wallops Island simulation had to be terminated after 22.5 minutes simulation time because of the constant buildup of the electric field strength. There is no mechanism within the model to relax the ever increasing electrical stresses. Nature takes care of the problem by initiating a lightning discharge. In order to be consistent, we realized that it was necessary for the model to be able to simulate a lightning discharge and its effects on the local charges and fields. Only when this capability was in place would the model be able to provide simulations of the mature and dissipating stages of a storm's electrical life. Since it is probably rare for the F106 to encounter a storm in its youngest stage, the ability to simulate the latter stages becomes paramount to further investigations. In order to conduct any further investigations into the storm electrical environment, which is a desired goal of the project, the model must be capable of simulating that environment throughout the life cycle of a storm.

4.2 Lightning Parameterization

These considerations led to investigating the question of incorporating (parameterizing) the lightning discharge in the SEM. We have two types of lightning to deal with; cloud-to-ground and intra-cloud. While intracloud lightning is the less well studied, it is also the most frequent to occur during a storm. It also seems, intuitively, to be the less complicated of the two to incorporate in the model and therefore was chosen to be examined first.

Without going into the arguments pro and con, we chose to adopt the philosophy of Kasemir (1960, 1984) whereby the overall intracloud lightning channel is electrically neutral. The charges that exist on the channel are the result of ionization along the channel and are not "gathered" from the surrounding cloud volume. When one deals with the simulation of the lightning discharge, which is a subgrid scale process in the SEM, four basic criteria must be established in order to account for the process: 1) initiation; 2) direction of propagation; 3) termination; and 4) charge redistribution. In attempting a first order approximation to the lightning discharge, the idea is to keep the processes involved as simple as possible while still trying to maintain a physically reasonable approach to the problem. Simplicity is also in order because the physical mechanisms involved in determining these criteria are poorly understood at this point. Thus, we have basically employed a single parameter approach to the first three processes mentioned above.

Recently Williams et al. (1985) have made a study of electrical discharges in polymethlymethacrylate (PMMA) which had been injected with electrons to form various space charge configurations. They found adequate scaled correlations to be able to relate the observed behavior of the discharges in the PMMA blocks to lightning discharges in thunderclouds. The paper focused on the local electric field strength and the space charge distribution as the factors controlling the extent and direction of propagation of the discharge channel. While the extent and magnitude of the space charge cloud are important in the morphology of the laboratory discharges, they identify the local electrostatic field as the single most important parameter in controlling such discharges. And although there is no direct justification for extrapolating their results to what takes place in thunderclouds, a scaling approach and the application of their model to specific thunderstorm situations argues in favor of accepting a possible correlation. As a result of their work and the concept of maintaining simplicity in the initial approach to the lightning parameterization, it was decided to use the local electric field as the parameter controlling the first three criteria in the above list.

As an initiation criterion, a threshold electric field was chosen with a value of 400 kV/m. Williams et al. (1985) quote a value of 500-1000 kV/m for a breakdown field in their Table 1. It has frequently been mentioned that the in-cloud breakdown field must be in the vicinity of 400 kV/m since the highest reliable in-cloud field measurements have peaked near that value. We feel that using this value in the model is reasonable because the value at a grid point represents the average value of the quantity within a grid box 200 m on a side (for this model) and this average would most likely consist of both higher and lower values.

The termination criterion was selected to be a critical field strength of 150 kV/m based on work done by Griffiths and Phelps (1976) involving the propagation of positive streamers in the laboratory. While serious questions can be raised about the appropriateness of extrapolating such a laboratory value to the atmosphere, we feel that it represents a reasonable threshold to use in the first approximation. It is true that the stepped leader which precedes a cloud-to-ground discharge appears to propagate through regions where the field strength does not exceed a few kilovolts per meter and such an extinction criterion as proposed above would not seem to be applicable; however, we are only dealing with the intracloud discharge at present.

In keeping with our single parameter formulation for the discharge process, we have chosen to use the electric field vector in determining the direction of the propagation path. Because the model domain is composed of grid points in a rectangular pattern, the lightning path is constrained to move either along the side of a grid box or along its diagonal, depending upon the direction of the electric field vector at that point. An algorithm has been developed which computes the angle of the field vector with respect to the vertical direction and

determines whether the path should be taken along the diagonal or the side. Even though the vector may be (and usually is) canted with respect to the vertical, the diagonal path is not chosen unless the canting exceeds a value of 22.5°. Because of these geometric constraints created by the use of a rectangular grid, the resulting lightning channel will probably be artificially relegated to a more vertical propagation path than would normally be observed in nature; however, for a first approximation, this seems to be a reasonable approach which can be improved upon as experience and increased knowledge dictate. For example, we recognize that the electric field vector at the tip of the propagating leader is important in determining the propagation direction; however, this is beyond the scope of a first order approximation and is the subject of a current research effort. Finally, since the initiation point of the channel is the point of highest electric field strength, the channel propagation is bi-directional from that point, moving both parallel and anti-parallel to the field vector and terminating when the field strength along each segment falls below the cutoff threshold.

In order to evaluate the effectiveness of these criteria, a test was conducted using model output from a simulation of the 19 July 1981 cloud which was observed in the vicinity of Miles City, MT, and produced a single intracloud lightning discharge (inferred from the electric field measurements of the NCAR/NOAA sailplane, see Dye et al., 1986). The initiation, propagation, and termination criteria as outlined above were applied to the model predicted state of the cloud at a time when the electric field was sufficient at some point in the domain to exceed the initiation threshold. From this point, the discharge path was computed in two directions following the electric field vector. The upward and downward paths continued until their termination thresholds were reached, at which point the discharge in that direction was stopped. The results of this process are shown in Fig. 6 which depicts the model calculated lightning channel superimposed on the ambient charge distribution (left panel) and the vertical electric field component (right panel). We can see that the discharge originates in the region of maximum vertical electric field which corresponds to a region of low net charge density. The discharge path is basically vertical following the dominant vertical electric field component and penetrates both the positive (upper) and negative (lower) charge centers. One should note, however, that the effect of the horizontal component of the electric field vector (not shown) becomes sufficient in the vicinity of the downward propagating part of the path so that the channel is deflected to the left as termination takes place. The total path length of the discharge channel in this instance is 2682 meters.

The parameterization of the lightning process must be completed by specifying the manner in which the charge created along the channel is redistributed into the environment. This aspect of the problem is being treated using ideas from Kasemir (1984) in which the charge per unit length along the channel is proportional to the difference between
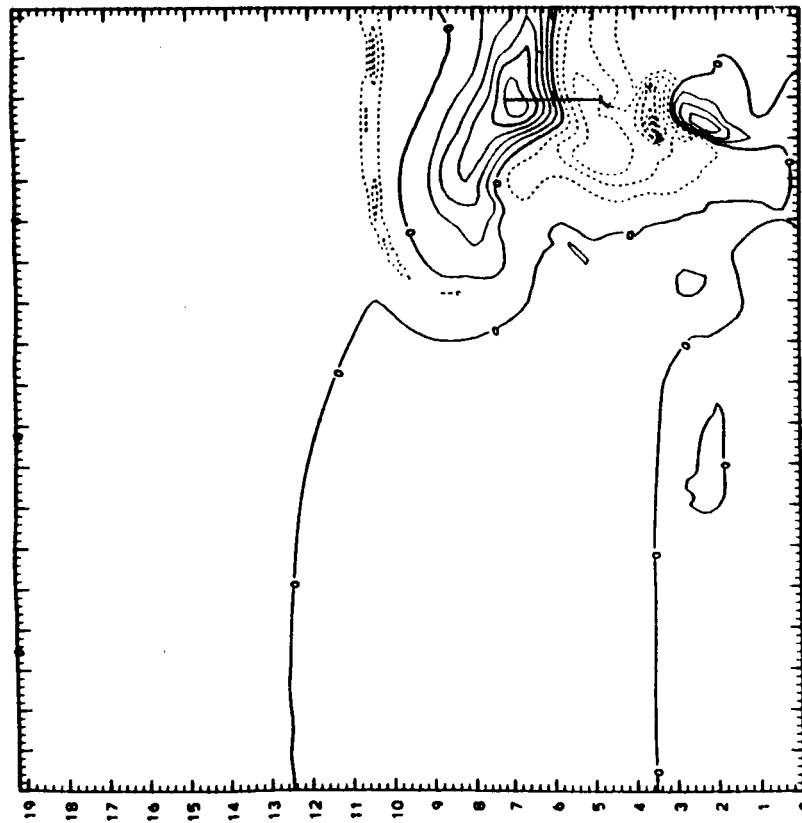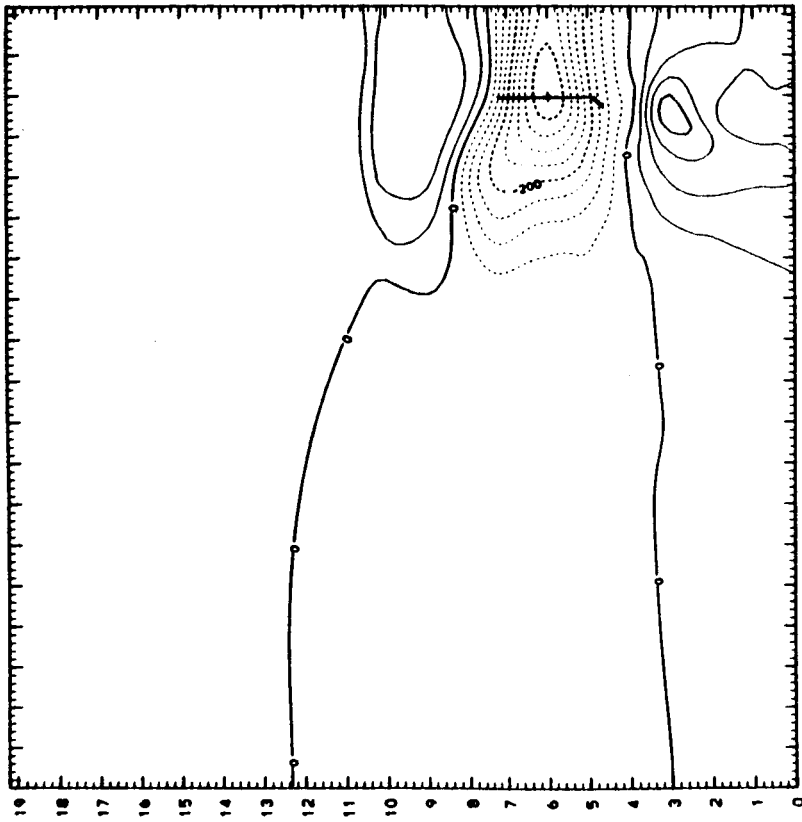
Fig. 6: Plots from the 19 July 1981 CCOPE case showing the model generated lightning channel superimposed on the model predicted net charge distribution (left panel) and vertical electric field component (right panel). The model domain is the same as in Fig. 1. The lightning channel is depicted as a vertical line segment centered at 6 km altitude and located 17 km from the left boundary. Note that the lower segment of the channel deviates from the vertical. In the left panel, the solid contours represent net positive charge and the dotted contours net negative charge. The contour interval is 0.9 nC/m^3 with the zero line indicated. In the right panel, the solid contours represent an upwardly directed electric field while the dotted contours represent a downwardly directed field. The contour interval is 50 kV/m and, again, the zero line is displayed.

29

the potential of the channel (defined as the potential at the point where the channel is initiated) and the ambient potential created by the cloud charge distribution. Such a scheme guarantees charge neutrality of the overall channel (if properly employed) and defines a systematic means by which charge can be distributed along the channel length. Since the total length of the channel is known, the total charge on each segment can be determined. Since intracloud lightning may be characterized by filamentary branching into the space surrounding the main channel, a scheme is also being devised to distribute the charge created along the channel in the space around the channel. This is also required in the model since the numerical schemes employed in solving the charge conservation equations are not capable of handling the shock of a line discontinuity which would be created if the charge were allowed to reside solely along the simulated channel. This distribution is being approximated using a Gaussian profile ($A\exp[-k(x-x_0)^2]$) to distribute the charge horizontally around the main channel. Here A represents the magnitude of the line charge density along the channel, x_0 is the x coordinate of the channel and k is a scaling coefficient chosen to cause the charge value to decrease to a specified fraction of its channel value at the edge of the distribution region. Since the minimum resolvable scale of a finite difference model of this type is twice the grid interval, it is necessary that a minimum of three grid points be involved in the definition of a distribution. In the case of the lightning charge distribution, we are starting with four grid points on either side of the channel path (1.6 km total width) to establish the distribution region. Experience will dictate modifications to this aspect of the problem which is the current focus of our research efforts.

5. CONCLUSIONS

The results of these investigations have given us some clues to the problem of the low altitude strike environment relevant to the F106 program. In addition, this work has raised several points that have lead to additional research thrusts of a pioneering nature.

With regard to the low level strike environment, the simulation of the Wallops Island case has shown that, within the limitations of the model physics, a region of high electric field strength does occur in the 15-20 kft altitude range. In the early developmental stage of the storm, this high field region is associated with the presence of graupel, and possibly turbulence, making it a region where flight operations would have to be restricted. However, it is entirely possible that at a later time in the storm's life cycle, such a high field region would continue to exist without being accompanied by threatening conditions. In addition, the Wallops Island simulation was characterized by little wind shear, leading to a nearly vertical development of the modeled storm. In a case where a stronger environmental shear were present, the high field region might not be concomitant with the presence of graupel or the graupel production might not be as heavy as in this case. Such speculation can only be resolved by testing the Wallops Island simulation further in time and running additional simulations of storms in which environmental shear is more significant.

The ability of the SEM to run a simulation further in time than is currently possible depends on the development of the lightning dis- charge parameterization. This is the pioneering research referred to above. No previous attempts to model the character of the actual lightning discharge channel have been made in the context of a large scale simulation model of this type. A first order approach to the problem has been undertaken in which the ambient electric field is the parameter used to determine the initiation, propagation, and termina- tion criteria for the simulated discharge. Using these criteria, we have been able to create a lightning channel within the context of an actual storm simulation. This channel, while not tortuous in nature, does exhibit some of the characteristics we would expect to see in an intracloud discharge.

The key to the continued development and use of the SEM as a research tool lies in the completion and improvement of the lightning parameterization scheme. This work involves the parameterization of the charge rearrangement associated with the lightning process, the development of a scheme to account for the cloud-to-ground discharge, and seeking improvements in the propagation and termination criteria. These three aspects of the parameterization scheme are currently being investigated.

ACKNOWLEDGMENTS

REFERENCES

Berry, E. X, 1968: Modification of the warm rain process. Preprints First Natl. Conf. Wea. Modif., Albany, NY, Amer. Meteor. Soc., 81-88.

Bigg, E. K., 1953: The supercooling of water. Proc. Phys. Soc. London, B66, 688-694.

Buser, O., and A. N. Aufdermaur, 1977: Electrification by collisions of ice particles on ice or metal targets. Electrical Processes in Atmospheres (eds. H. Dolazalek and R. Reiter), Steinkopff-Verlag, Darmstadt, 294-301.

Chen, C-H., and H. D. Orville, 1980: Effects of mesoscale convergence on cloud convection. J. Appl. Meteor., 19, 256-274.

Chiu, C. S., 1978: Numerical study of cloud electrification in an axisymmetric, time-dependent cloud model. J. Geophys. Res., 83, 5025-5049.

Crowley, W. P., 1968: Numerical advection experiments. Mon. Wea. Rev., 96, 1-11.

Dye, J. E., J. J. Jones, W. P. Winn, T. A. Cerni, B. Gardiner, D. Lamb, R. L. Pitter, J. Hallett and C. P. R. Saunders, 1986: Early electrification and precipitation development in a small, isolated Montana cumulonimbus. J. Geophys. Res., 91, 1231-1247.

Fisher, B. D., and J. A. Plumer, 1984: Lightning attachment patterns and flight conditions experienced by the NASA F-106B airplane from 1980-1983. Presented at AIAA 22nd Aerospace Sciences Meeting, Reno, NV.

_____, P. W. Brown and J. A. Plumer, 1986: Summary of NASA storm hazards lightning research, 1980-1985. Presented at the Intnl. Conf. Lightning and Static Electricity, Dayton, OH.

Fletcher, N. H., 1962: The Physics of Rainclouds. Cambridge Univ. Press, NY. 390 pp.

Gaskell, W., and A. J. Illingworth, 1980: Charge transfer accompanying individual collisions between ice particles and its role in thunderstorm electrification. Quart. J. Roy. Meteor. Soc., 106, 841-854.

Gish, O. H., 1944: Evaluation and interpretation of the columnar resistance of the atmosphere. Terr. Magn. Atmos. Elect., 49, 159-168.

Griffiths, R. F., and C. T. Phelps, 1976: The effects of air pressure and water vapour content on the propagation of positive corona streamers and their implications to lightning initiation. <u>Quart. J. Roy. Meteor. Soc.</u>, <u>102</u>, 419.

Gross, G. W., 1982: Role of relaxation and contact times in charge separation during collisions of precipitation particles with ice targets. <u>J. Geophys. Res.</u>, <u>87</u>, 7170-7178.

Hallett, J., and C. P. R. Saunders, 1979: Charge separation associated with secondary ice crystal production. <u>J. Atmos. Sci.</u>, <u>36</u>, 2230-2235.

Helsdon, J. H., Jr., 1980: Chaff seeding effects in a dynamical-electrical cloud model. <u>J. Appl. Meteor.</u>, <u>19</u>, 1101-1125.

_____, R. D. Farley and H. D. Orville, 1984: A numerical modeling study of ice electrification mechanisms in a Montana cloud. <u>Preprints VIIth Intnl. Conf. Atmos. Elec.</u>, Albany, NY, Amer. Meteor. Soc., 174-177.

Jayaratne, E. R., C. P. R. Saunders and J. Hallett, 1983: Laboratory studies of the charging of soft-hail during ice crystal interactions. <u>Quart. J. Roy. Meteor. Soc.</u>, <u>109</u>, 609-630.

Jennings, S. G., 1975: Charge separation due to water drop and cloud droplet interactions in an electric field. <u>Quart. J. Roy. Meteor. Soc.</u>, <u>101</u>, 227-223.

Kasemir, H., 1960: A contribution to the electrostatic theory of a lightning discharge. <u>J. Geophys. Res.</u>, <u>65</u>, 1873-1878.

_____, 1984: Theoretical and experimental determination of field, charge, and current on an aircraft hit by natural or triggered lightning. Presented at the Intnl. Aerospace and Ground Conf. on Lightning and Static Electricity, Orlando, FL.

Kessler, E., 1969: On the distribution and continuity of water substance in atmospheric circulations. <u>Meteor. Monogr.</u>, <u>10</u>, No. 32. 84 pp.

Kuettner, J. P., Z. Levin and J. D. Sartor, 1981: Thunderstorm electrification--inductive or non-inductive? <u>J. Atmos. Sci.</u>, <u>38</u>, 2470-2484.

Latham, J., and B. J. Mason, 1961: Generation of electric charge associated with the formation of soft hail in thunderclouds. <u>Proc. Roy. Soc.</u>, <u>A260</u>, 537-549.

_____, and R. Warwicker, 1980: Charge transfer accompanying the splashing of supercooled raindrops on hailstones. Quart. J. Roy. Meteor. Soc., 106, 559-568.

Leith, C. E., 1965: Numerical simulation of the earth's atmosphere. Methods in Computation Physics, Vol. 4, Applications in Hydrodynamics, Academic Press.

Lin, Y-L., R. D. Farley and H. D. Orville, 1983: Bulk parameterization of the snow field in a cloud model. J. Climate Appl. Meteor., 22, 1065-1092.

Liu, J. Y., and H. D. Orville, 1969: Numerical modeling of precipitation and cloud shadow effects on mountain-induced cumuli. J. Atmos. Sci., 26, 1283-1298.

Mazur, V., B. D. Fisher and J. C. Gerlach, 1984: Conditions for lightning strikes to an airplane in a thunderstorm. Presented at the AIAA 22nd Aerospace Sciences Meeting, Reno, NV.

Muller-Hillebrand, D., 1954: Charge generation in thunderstorms by collision of ice crystals with graupel falling through a vertical electric field. Tellus, 6, 367-381.

Musil, D. J., 1970: Computer modeling of hailstone growth in feeder clouds. J. Atmos. Sci., 27, 474-482.

Orville, H. D., 1965: A numerical study of the initiation of cumulus clouds over mountainous terrain. J. Atmos. Sci., 22, 684-699.

_____, and F. J. Kopp, 1977: Numerical simulation of the life history of a hailstorm. J. Atmos. Sci., 34, 1596-1618.

Paluch, I. R., and J. D. Sartor, 1973: Thunderstorm electrification by the inductive charging mechanism: I. Particle charges and electric fields. J. Atmos. Sci., 30, 1166-1173.

Reynolds, S. E., M. Brook and M. F. Gourley, 1957: Thunderstorm charge separation. J. Meteor., 14, 426-436.

Rudolph, T., and R. A. Perala, 1985: Studies in increasing the probability that the NASA F-106B thunderstorm research aircraft will intercept low altitude lightning strikes. Tech. Rpt. EMA-85-R-24. 101 pp.

_____, _____, P. M. McKenna and S. L. Parker, 1984: Investigations into the triggered lightning response of the F-106B thunderstorm research aircraft. Tech. Rpt. EMA-85-R-02.

Sartor, J. D., 1961: Calculations of cloud electrification based on a general charge separation mechanism. J. Geophys. Res., 66, 831-843.

_____, 1967: The role of particle interactions in the distribution of electricity in thunderstorms. J. Atmos. Sci., 24, 601-615.

_____, 1981: Induction charging of clouds. J. Atmos. Sci., 38, 218-220.

Saunders, P. M., 1957: The thermodynamics of saturated air: A contribution to the classical theory. Quart. J. Roy. Meteor. Soc., 83, 342-350.

Shewchuk, S. R., and J. V. Iribarne, 1971: Charge separation during splashing of large drops on ice. Quart. J. Roy. Meteor. Soc., 97, 272-282.

Shreve, E. L., 1970: Theoretical derivation of atmospheric ion concentrations, conductivity, space charge density, electric field and generation rate from 0 to 60 km. J. Atmos. Sci., 27, 1186-1194.

Takahashi, T., 1978: Riming electrification as a charge generation mechanism in thunderstorms. J. Atmos. Sci., 35, 1536-1548.

Telford, J. W., and P. B. Wagner, 1979: Electric charge separation in severe storms. Pure Appl. Geophys., 117, 891-903.

Tzur, I., and Z. Levin, 1981: Ions and precipitation charging in warm and cold clouds as simulated in a one-dimensional, time-dependent model. J. Atmos. Sci., 38, 2444-2461.

Vonnegut, B., 1955: Possible mechanism for the formation of electricity. Geophys. Res. Pap., No. 42, Air Force Cambridge Res. Center, MA, 169-181.

Williams, E. R., C. M. Cooke and K. A. Wright, 1985: Electrical discharge propagation in and around space charge clouds. J. Geophys. Res., 90, 6059-6070.

Wilson, C. T. R., 1929: Some thundercloud problems. J. Franklin Inst., 208, 1-12.

Wisner, C. E., H. D. Orville and C. Myers, 1972: A numerical model of a hailbearing cloud. J. Atmos. Sci., 29, 1160-1181.

Workman, E. J., and S. E. Reynolds, 1948: A suggested mechanism for the generation of thunderstorm electricity. Phys. Rev., 74, 709.

_____, and _____, 1950: Electrical phenomena occurring during the freezing of dilute aqueous solutions and their possible relationship to thunderstorm electricity. Phys. Rev., 78, 254-259.